

# High Voltage Test Apparatus for a Neutron EDM Experiment and Lower Limit on the Dielectric Strength of Liquid Helium at Large Volumes

J. C. Long \*

*LANSCE-NS, Los Alamos National Laboratory, Los Alamos NM 87545 USA*

P. D. Barnes, J. G. Boissevain, D. J. Clark, M. D. Cooper  
J. J. Gomez, S. K. Lamoreaux, R. E. Mischke, S. I. Penttila

*Physics Division, Los Alamos National Laboratory, Los Alamos NM 87545 USA*

---

## Abstract

A new search for a permanent electric dipole moment (EDM) of the neutron is underway using ultracold neutrons produced and held in a bath of superfluid helium. Attaining the target sensitivity requires maintaining an electric field of several tens of kilovolts per centimeter across the experimental cell, which is nominally 7.5 cm wide and will contain about 4 liters of superfluid. The electrical properties of liquid helium are expected to be sufficient to meet the design goals, but little is known about these properties for volumes and electrode spacings appropriate to the EDM experiment. Furthermore, direct application of the necessary voltages from an external source to the experimental test cell is impractical. An apparatus to amplify voltages in the liquid helium environment and to test the electrical properties of the liquid for large volumes and electrode spacings has been constructed. The device consists of a large-area parallel plate capacitor immersed in a 200 liter liquid helium dewar. Preliminary results show the breakdown strength of normal state liquid helium is at least  $90 \text{ kV cm}^{-1}$  at these volumes, at the helium vapor pressure corresponding to 4.38 K. These fields hold for more than 11 hours with leakage currents less than 170 pA (about 20% of the maximum tolerable in the EDM experiment). The system is also found to be robust against anticipated radiation backgrounds. Preliminary results for superfluid show that fields of at least  $30 \text{ kV cm}^{-1}$  can be sustained at the volumes required for the EDM experiment, about 60% of the design goal. These results are likely limited by the low pressure that must be maintained above the superfluid bath.

*Key words:* Liquid helium, Superfluid helium (He II), Dielectric properties, Instrumentation, Power applications

## 1 Introduction

The search for a permanent electric dipole moment (EDM) of the neutron has been the subject of experimental investigations for nearly 50 years [1]. It has generally been of interest as a test of the discrete space-time symmetries, and has more recently emerged as one of the most sensitive tests of physics beyond the Standard Model [2].

A nonzero EDM ( $d_e$ ) would be a signal of time-reversal symmetry violation and has yet to be observed. The most sensitive upper limit to date,  $d_e \leq 6.3 \times 10^{-26}$  e-cm (90% C. L.), is derived from experiments performed on ultracold neutrons (UCN) [3]. UCN have kinetic energies of a few hundred nanoelectron volts—less than the Fermi potential of many substances—and are easily trapped. The neutron velocities in these experiments are small and randomized, which is very advantageous for the suppression of systematic effects associated with motional magnetic fields. A new EDM search, with potentially unprecedented sensitivity, is underway using UCN produced via the superthermal process (the downscattering of cold neutrons by phonons) in a superfluid helium bath and subsequently held in the bath [2,4,5].

The statistical sensitivity  $\sigma_d$  of these experiments can be approximated by the expression:

$$\sigma_d \geq \frac{\hbar}{E\sqrt{TNt}} \tag{1}$$

where  $\hbar$  is Planck's constant,  $E$  is the electric field to which the neutron sample is exposed,  $T$  is the experimental measurement cycle time,  $N$  is the number of neutrons sampled per cycle, and  $t$  is the cumulative storage time. For the experiment under construction, the target neutron sample is  $N \sim 1 \times 10^6$ , using neutrons downscattered from a dedicated beam at the Spallation Neutron Source (SNS) under construction at the Oak Ridge National Laboratory. The target sample time is  $T \sim 500$  s, which is expected to be determined primarily by the beta decay lifetime of the UCNs held in the very inert environment of the superfluid bath. A total of about  $2 \times 10^5$  measurement cycles are expected, for a cumulative storage time of  $\sim 10^8$  s. The target electric field is  $50 \text{ kV cm}^{-1}$ .

---

\* Corresponding author. Present address: Indiana University Cyclotron Facility, Bloomington IN 47408 USA

The dielectric properties of liquid helium (LHe) are expected to be sufficient to meet the electric field design parameter, however, very little is known about these properties for volumes and electrode spacings appropriate to the experiment. The reference design calls for a measurement cell with a volume of about 4 liters of superfluid (SF) LHe, positioned between a set of parallel-plate high voltage (HV) electrodes of nominal area  $A_e = 2000 \text{ cm}^2$ . The electrode spacing and hence the cell width is nominally  $z_e = 7.5 \text{ cm}$ .

The existing data for the electric breakdown strength of LHe are summarized in Fig. 1, which is adapted from [6]. At electrode spacings below 1 mm, breakdown fields well in excess of  $300 \text{ kV cm}^{-1}$  are observed. This reduces to  $150 \text{ kV cm}^{-1}$  for gaps of 1 cm, however. Furthermore, as of the inception of the project described in this work, reliable data for larger spacings were not available in the literature. The extrapolation of the breakdown voltage to larger spacings suggested in [6] is  $V_b = Cz^{0.8}$ , where  $V_b$  is in  $\text{kV cm}^{-1}$ ,  $z$  is in cm and  $C = 136 \text{ kV cm}^{-0.8}$ . This extrapolation is illustrated in Fig. 1, and suggests an expected breakdown field of about  $95 \text{ kV cm}^{-1}$  at the nominal electrode spacing. This is well above the design target, if an extrapolation of nearly an order of magnitude in the electrode spacing is to be trusted.

As emphasized in [6], however, electric breakdown in cryogenic liquids is influenced by many factors, including the volume of stressed liquid. In particular, the expression

$$E_{b2} = E_{b1} \left( \frac{S_2}{S_1} \right)^{-1/m} \quad (2)$$

is cited in [6] as an order-of-magnitude estimate for the reduction in breakdown field  $E_{b2}$  as a function of the overall stressed volume  $S_2$ , relative to reference values  $E_{b1}$  and  $S_1$ . Suggested values of the exponent  $1/m$  range in the literature from about 0.08 to 0.17. According to [7], the data in Fig. 1 are obtained from an experiment with spherical electrodes of radius  $r = 3.1 \text{ cm}$ . Assuming circular plate electrodes of the same radius for simplicity and the sake of an order-of-magnitude estimate, the stressed volume  $S_1$  is given by  $\pi r^2 z$ , where  $z$  is the separation. Substituting this and the relation  $S_2 = A_e z$  for the stressed volume in the EDM experiment into Eq. 2 yields an estimate for the expected reduced breakdown field between the EDM electrodes relative to the experiment in [7]. As the breakdown voltage scales with the field for the parallel plate electrodes, scaling the extrapolated curve in Fig. 1 by  $(S_2/S_1)^{-1/m}$  yields the plots labeled “size effect limits” in that figure. This is the modified expectation for the breakdown voltage in the EDM experiment. The upper and lower bounds correspond to the exponent  $1/m = 0.08$  and 0.17, respectively, suggesting a wide possible range in the vicinity of the design voltage (about 375 kV for the 7.5 cm electrode gap).

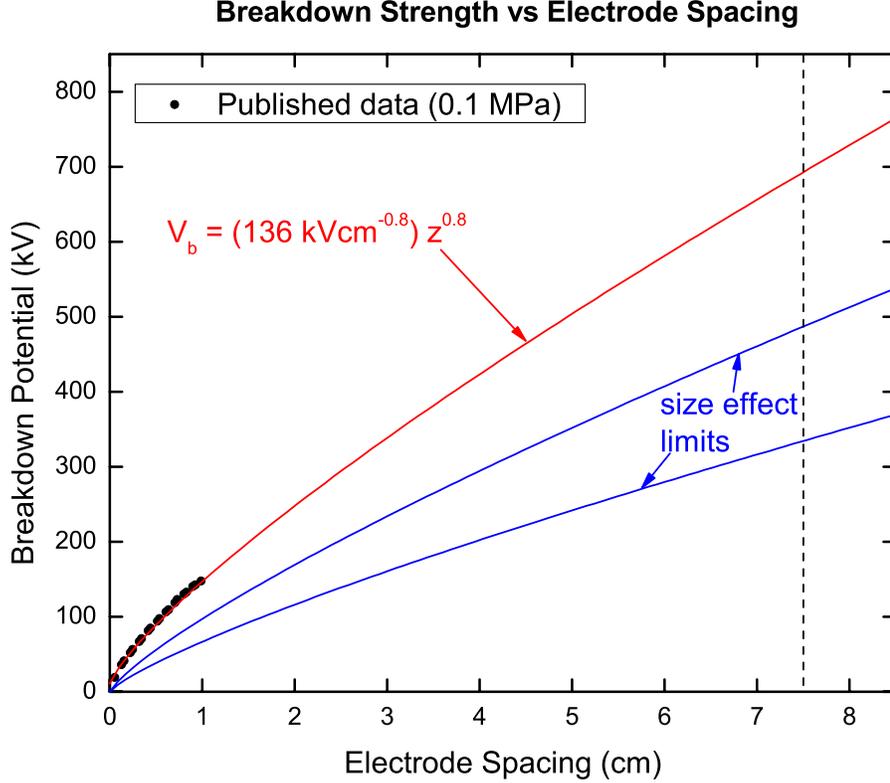


Fig. 1. Breakdown voltage vs. electrode spacing for saturated LHe. The black dots are existing experimental data from [7]. The extrapolation suggested in [6] is shown, together with the further reduction (“size effect limits”) expected in the EDM experiment due to the larger volume of LHe relative to that in [7].

Additional factors influencing breakdown cited in [6] include surface roughness, stressing time, and liquid pressure, for which understanding and predictability are partial at best. Furthermore, the foregoing data and discussion apply only to saturated LHe in the normal state. Evidence presented in [6] suggests additional reduction in breakdown strength for the SF state relevant to the EDM experiment. This state of affairs motivates a direct experimental assessment of the dielectric properties of LHe at large volumes and electrode spacings, and in the SF state.

In addition to the breakdown strength of LHe at large volumes, several other engineering parameters are of interest to the neutron EDM experiment. Of greater interest than the pure breakdown strength is a stable operating point, defined as the maximum voltage attainable with a breakdown probability of at most a few percent over the entire anticipated integration time of the experiment ( $\sim 10^8$  s). This value will ostensibly be chosen as the experimental operating voltage in order to protect the EDM detection system, which will be SQUID-based and likely damaged in the event of a spark discharge. The elec-

tric field stability over time  $\Delta E_t$  is also of interest, with a target of  $\Delta E_t \leq 1\%$  required over the course of a measurement cycle to suppress false EDM signals generated by stray magnetic fields [5]. This translates into a leakage current upper limit of about 1 nA for the EDM HV system. The electric field uniformity  $\Delta E_V$  is of similar importance, with a target of  $\Delta E_V \leq 1\%$  required over the experimental cell volume to further control systematics associated with motional magnetic fields [5,8].

Finally, direct application of the required voltages from an external power source would require electrical feedthroughs impractically large for the cryogenic environment. Therefore, an apparatus has been designed to test a simple in-situ amplification mechanism in addition to testing the parameters listed above. In this mechanism, a small initial potential is used to charge a variable, parallel-plate capacitor in the LHe volume. The potential source is then disconnected and the voltage amplified by separating the plates and reducing the capacitance. In the reference design of the final version of the EDM experiment, the amplifier (variable) capacitor is connected in parallel to a pair of fixed capacitors (with the nominal electrode dimensions mentioned above) that flank the actual measurement cells [5]. In the test system described here, only the variable capacitor has been prototyped, which should be sufficient to test the dielectric properties of LHe and to verify the amplification principle.

## 2 Apparatus

### 2.1 Central Volume

The design chosen for the central volume of the test apparatus is shown in Fig. 2. It consists of a parallel-plate capacitor with cylindrical electrodes, mounted horizontally on the central axis of a cylindrical LHe tank.

The electrodes of the parallel-plate capacitor are shown in Fig. 3 and their dimensions listed in Table 1. Both electrodes consist of hollow cylindrical shells of type 6061 aluminum. Two small holes are bored into the outer edges of each electrode to allow for filling with LHe during operation.

The HV electrode is fixed to the inner surface of the central volume end flange with three insulating stand-offs. The movable ground electrode has the same diameter as the HV electrode but is narrower in profile. An aluminum rod attaches to the rear of the electrode and connects to a welded bellows for position control along the axis normal to the electrode surfaces.

The fixed HV electrode is charged via a second movable electrode mounted

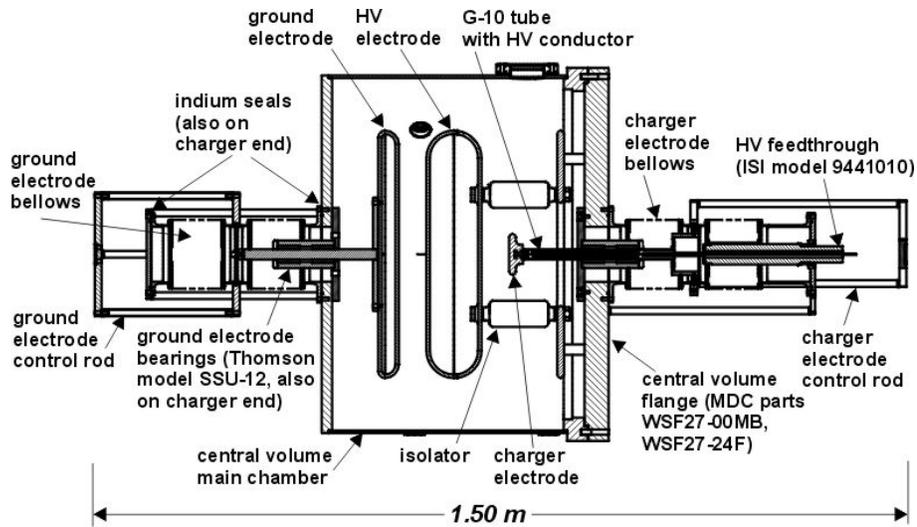


Fig. 2. Assembly drawing (elevation, to scale) of HV test system central volume.

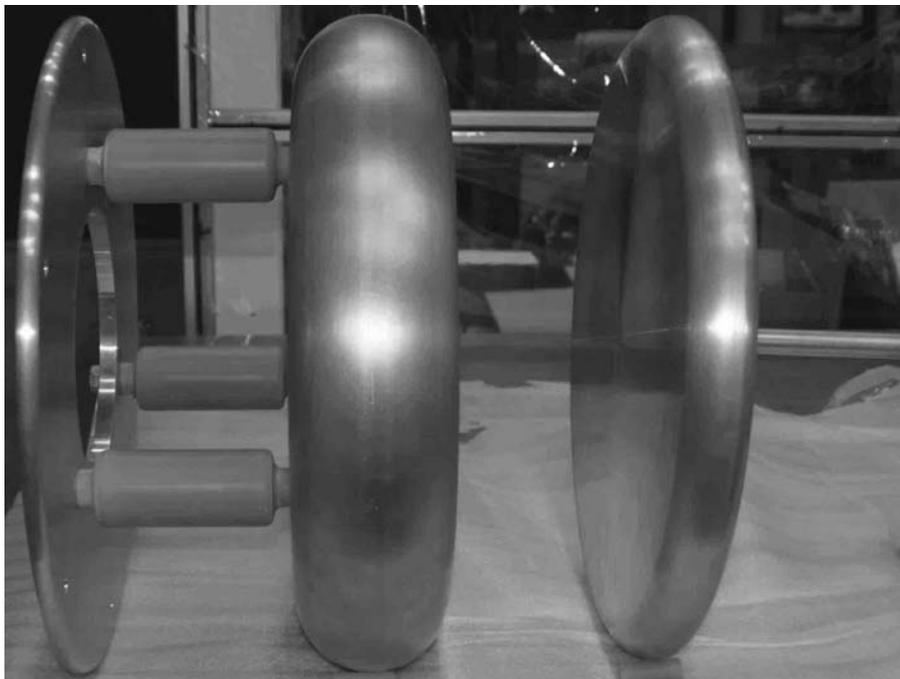


Fig. 3. HV test system electrodes before installation in the central volume. The HV electrode is in the center. It is fixed to the solid aluminum plate at the left with three G-10 insulating stand-offs. The plate is in turn bolted (and grounded) to the inner surface of the central volume flange.

on the side opposite the ground electrode. It consists of a solid type 6061 aluminum disk with rounded edges. The electrode is attached to a G-10 tube which connects to a second bellows for position control. A steel spring attaches to the back of the electrode and leads out of the HV system through the G-10

Table 1  
 HV test system electrode dimensions

Surface roughness, all electrodes	1.6 $\mu\text{m}$ rms
Surface flatness, all electrodes	0.005 cm
Diameter, HV and ground electrodes	45.8 cm
Diameter, charger electrode	7.6 cm
Wall thickness, HV and ground electrodes	0.6 cm
Length, HV electrode	10.2 cm
Length, ground electrode	2.5 cm
Length, charger electrode	1.3 cm
Edge curvature radius, HV electrode	5.1 cm
Edge curvature radius (average), ground electrode	1.9 cm
Edge curvature radius, charger electrode	0.64 cm
Length, HV electrode insulators	14.0 cm
Diameter, HV electrode insulators	5.1 cm

tube to an external power supply.

The central LHe volume (Table 2) of the test system consists of a stainless steel vessel closed with a wire-seal flange. The flange is a standard part except that the number of bolt holes has been doubled to help insure against superleaks, and is itself a prototype component to be tested for the final version of the EDM experiment. To minimize heat loads, the central volume is held in place with a sling made from two Kevlar ropes anchored in the surrounding copper radiation shield (Sec. 2.2) with specially-designed jigs.

Control of the movable ground and charger electrodes is provided by welded bellows attached to either end of the central volume with indium seals. Each bellows consists of two welded sections attached in series with a rigid center ring between the sections (Fig. 4). Rods attached to the movable electrodes exit the central volume via bearings mounted in G-10 blocks, and connect to the inner surfaces of the center rings. During operation, the bellows fill with LHe through a series of holes in the G-10 blocks. The bearings are standard parts with stainless steel balls in plastic casings from which all oil is removed before installation. Friction is a concern and operation of the apparatus tests whether the LHe itself can serve as an adequate lubricant. The bellows are operated by control rods attached to the exteriors of the center rings, so that one bellows section extends while the other compresses, maintaining a constant

Table 2  
 HV test system central LHe volume dimensions

Inner length (excluding flange spaces)	44.0 cm
Inner diameter (excluding flange spaces)	66.0 cm
Side wall thickness	0.5 cm
Welded end wall thickness	0.6 cm
Wire-seal flange thickness	4.4 cm
Bellows length (HV side)	37.3 cm
Bellows mean inner diameter (HV side)	10.8 cm
Mass	$\approx 300$ kg
LHe volume (including flange spaces and bellows)	180 l

LHe volume in the bellows.

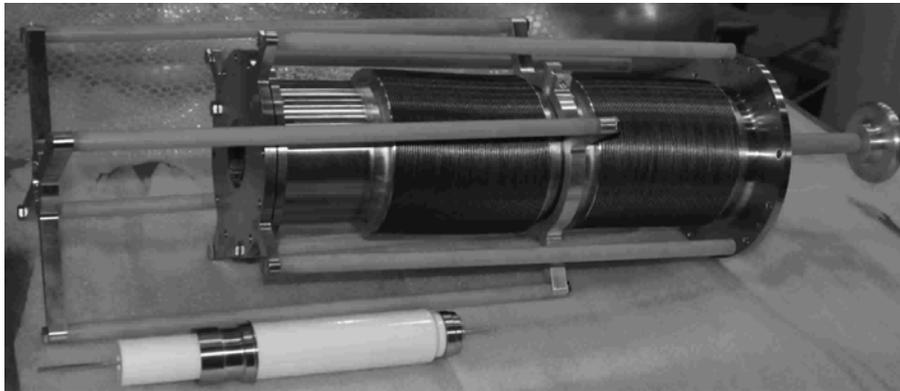


Fig. 4. Bellows system for position control of charger electrode, before attachment to HV test system central volume. The charger electrode protrudes from the right end. The ceramic feedthrough used to bring the initial HV potential into the LHe volume can be seen in the foreground before being welded into place in the small hole in the left end-cap of the bellows assembly.

## 2.2 Vacuum System

The complete design for the EDM HV test system is shown in Fig. 5. The central volume is supplied with LHe via an auxiliary 20-liter cryostat mounted to the top. The central and upper LHe volumes are surrounded by thin-walled copper radiation shields, cooled to about 100 K via thermal contact with a 10-liter liquid nitrogen reservoir surrounding the upper volume. All LHe volumes and radiation shields are wrapped with 15–20 layers of aluminized

Mylar superinsulation.

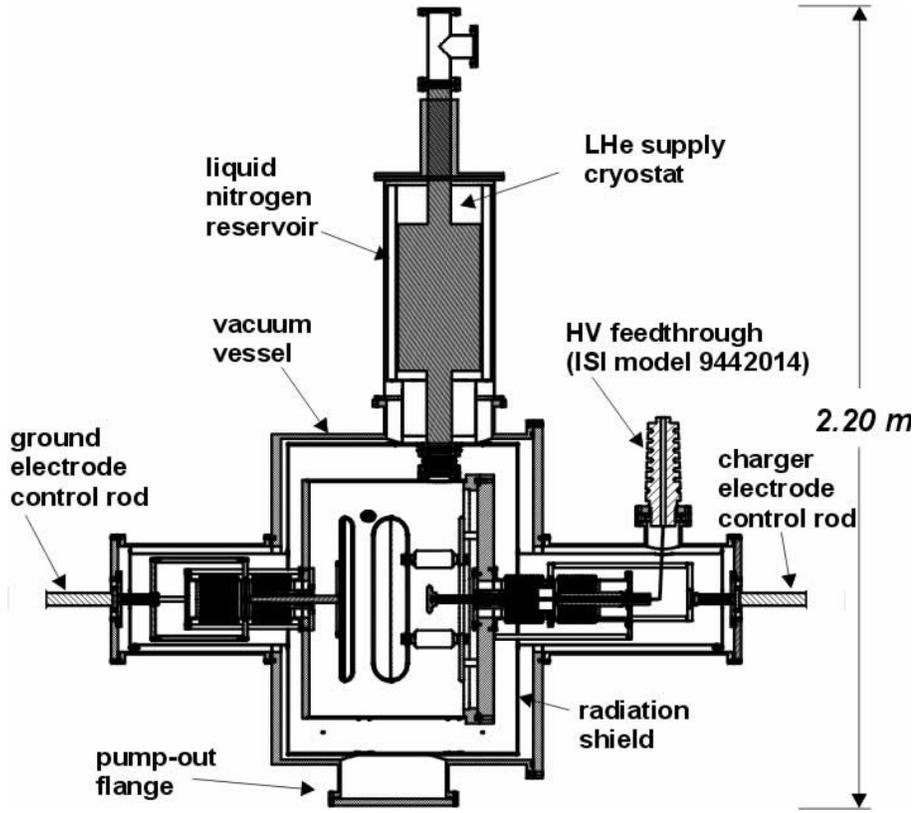


Fig. 5. Assembly drawing (to scale) of HV test system vacuum volume. Rods for electrode motion control exit the ends of the vacuum system via external bellows and connect to automated linear slides (Fig. 6).

The entire assembly is placed inside a  $\sim 1 \text{ m}^3$  aluminum vacuum chamber. The chamber can typically be maintained at  $1 \times 10^{-6}$  torr at room temperature with a  $\sim 500 \text{ l s}^{-1}$  turbomolecular pump mounted at the bottom. The vacuum has been observed to improve by more than an order of magnitude with cryopumping.

The HV interface between air and LHe consists of two standard ceramic feedthroughs (Table 3). One feedthrough is mounted to a flange on the outer arm of the vacuum system above the charger electrode control bellows (Figs. 5 and 6), and a smaller feedthrough is welded into the end-cap of the HV bellows (Fig. 4). The upper ceramic portion of the small feedthrough protrudes completely into the LHe volume (Fig. 2); operation of the system tests its performance in the cryogenic environment. The bottom tips of the feedthrough conductors are soldered together, and the upper tip of the smaller feedthrough is soldered to a stainless steel spring. The spring attaches to the charger electrode through the G-10 tube.

The control rods for the ground and charger electrodes attach to the inner end-

Table 3  
HV feedthrough parameters

Air–vacuum feedthrough ceramic length	29.2 cm
Air–vacuum feedthrough ceramic outer diameter	8.9 cm
Air–vacuum feedthrough breakdown rating	100 kV
Vacuum–LHe feedthrough ceramic length	24.0 cm
Vacuum–LHe feedthrough ceramic outer diameter	3.8 cm
Vacuum–LHe feedthrough breakdown rating	40 kV

caps of small welded bellows mounted externally to either end of the vacuum system (Fig 6). The external bellows are in turn attached to screw–driven linear slides controlled by servo motors. With this system, the minimum gap between the HV and ground (charger) electrodes can be adjusted from 0 to 10 cm (7 cm) over a wide range of speeds, with a nominal accuracy of less than 0.1 mm. The gap between the electrode surfaces is viewable through a series of 5 cm diameter quartz view ports in the side walls of the central volume and vacuum chamber.

### 2.3 Data Acquisition

The view ports are designed to permit the eventual use of a laser to monitor the electric field via the Kerr effect in the LHe [9]. For the present studies, the small charger electrode is used as a capacitive probe of the voltage between the HV and movable ground electrodes. The equivalent circuit of the HV apparatus is shown in Fig. 7. In a typical HV amplification and measurement cycle, a 50 kV HV power supply is connected to the air–vacuum feedthrough via a 6 m cable. The gap between the ground and HV electrodes is set to an initial value of a few millimeters. The charger electrode is brought into contact with the HV electrode, and a potential of a few tens of kV is applied. With the power supply still engaged, the charger is retracted to a reference position several centimeters behind the HV electrode. The power supply is switched off, and the cable is moved from the power supply output to the input of a charge-sensitive meter. The meter records the change in charge  $\Delta Q_C$  on the charger electrode as the gap between the HV and ground electrode is increased to amplify the voltage.

From the diagram in Fig. 7, the change in voltage across the variable capaci-

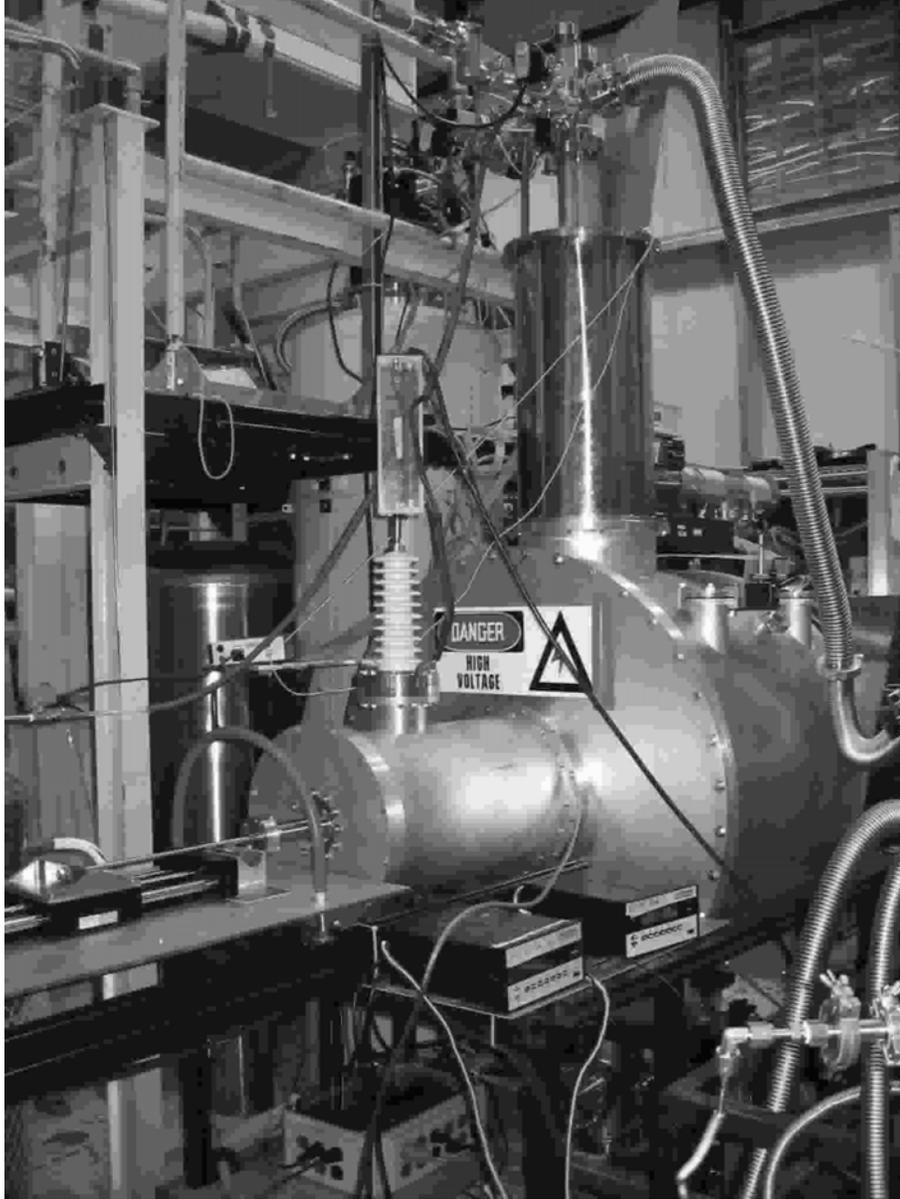


Fig. 6. Fully assembled HV test system. The vacuum system arm surrounding charger electrode control bellows is visible in the foreground, with the air-vacuum HV feedthrough attached at the top. The small external bellows, control rod, and motor-driven linear slide for the charger electrode control are visible in front of the arm. The supply cryostat is visible on top of the main vacuum volume. The flexible tubing for pumping on the LHe bath stretches down from the top of the supply cryostat.

tance  $C_{HG}$  is given by:

$$\Delta V_{HG} = \Delta Q_C \left( \frac{1}{C_{HC}} + \frac{1}{C_{CF} + C_{MF}} \right) \quad (3)$$

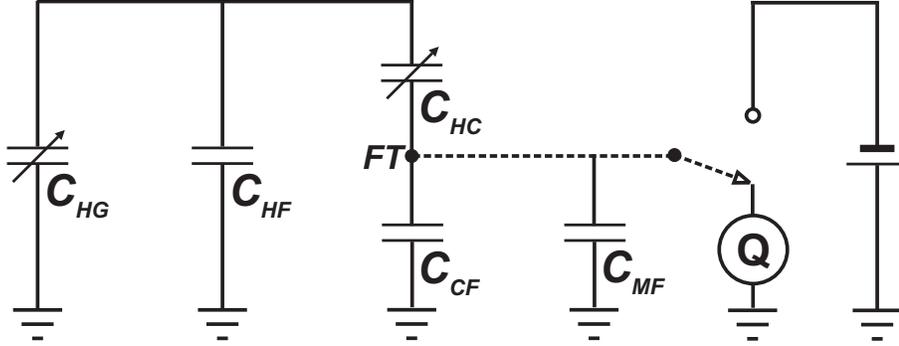


Fig. 7. HV test system equivalent circuit. The point labeled  $FT$  corresponds to the upper tip of the air-vacuum feedthrough and forms the output of a capacitive divider. One side of the divider is formed by the capacitance between the HV and ground electrode ( $C_{HG}$ ), in series with the capacitance of the HV and charger electrode ( $C_{HC}$ ). The other side is formed by the fixed capacitance of the charger electrode and ground ( $C_{CF}$ ).  $C_{HF}$  is the fixed capacitance of the HV electrode with respect to ground. When the system is connected to a charge-sensitive meter ( $Q$ ),  $C_{CF}$  is in parallel with the fixed capacitance of the cable plus the meter with respect to ground ( $C_{MF}$ )

In practice, a sensitive current amplifier is used in place of a charge meter and the output is integrated over time during the measurement.

The complete schematic of the HV test system is shown in Fig. 8. A  $10\text{ M}\Omega$  resistor is put in series with the cable to provide some protection for the electronics from spark discharges. For data acquisition after charging, the cable is switched manually to the current amplifier. The current amplifier is read out with a PC-based digital-to-analog converter, at a software-limited rate (for this work) of  $130\text{ Hz}$ . For diagnostic purposes during cool-down, temperatures are monitored at various points on the central volume and radiation shield with a series of silicon diode sensors. During operation, LHe temperature is controlled by pumping on the main bath with a  $25\text{ l s}^{-1}$  (air) oil-sealed mechanical pump (occasionally boosted to  $\sim 40\text{ l s}^{-1}$  with a roots blower), and temperature is inferred from the He vapor pressure. The motors running the linear slides are PC-controlled via servo drives. Initial HV-ground electrode spacing is measured with a surveyor's transit focused on the electrode surfaces through the view ports.

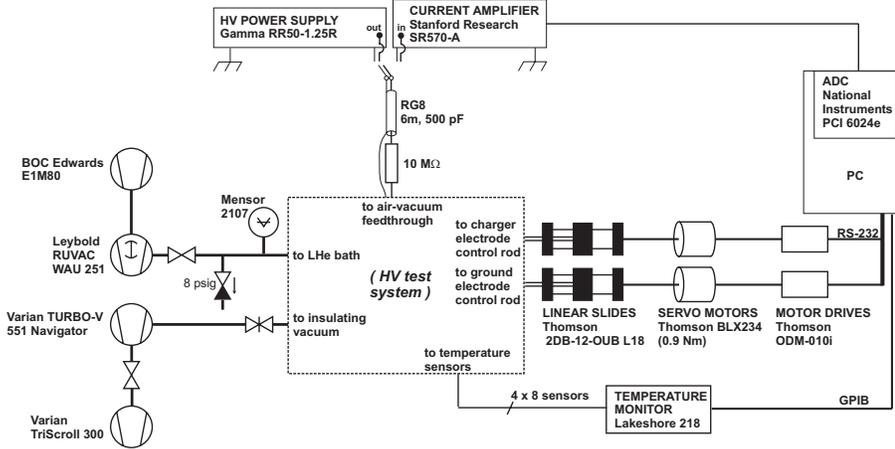


Fig. 8. Basic schematic of complete system.

### 3 Results

#### 3.1 Cryogenic Performance and HV Test Conditions

Conduction cool-down of the radiation shields from room temperature to 100 K takes approximately 72 hr. Liquid nitrogen pre-cooling of the central volume is done in steps over the course of about 12 hr so as to minimize thermal gradients across the large wire-seal flange. This is further aided by spraying the liquid in radial jets onto the side walls of the central volume and relying on the thermal conductivity of the walls to cool the flange uniformly. Initial filling of the LHe main volume from a standard 500 l storage dewar takes approximately 45 min. SF production is achieved by pumping on the main bath. To ensure quantities of SF sufficient to completely immerse the electrodes are obtained, both the LHe supply and HV system volumes are pre-cooled via pumping to just above the lambda point. The HV system bath is then topped off with LHe at low vapor pressure ( $\sim 90$  torr) before being pumped to below the lambda point.

During normal operation, typical LHe boil-off rates of  $2\text{--}3 \text{ l hr}^{-1}$  (liquid) are observed. This rate corresponds to a total heat load of 1.6- 2.3 W, likely dominated by conduction through the upper neck of the small supply cryostat. No appreciable changes in the insulating vacuum are observed (resolution  $\sim 10^{-7}$  torr) during SF production or operation, indicating the feasibility of using the standard wire-seal flange technology for large volumes of SF in the EDM cryostat. No degradation in the range and precision of the position control of the electrodes is observed at cryogenic temperatures. However, moving the electrodes requires significantly higher ( $\sim$  factor 3) torque from the motors than at room temperature. While the reason is unclear, this factor remains constant over the course of operation of the system, suggesting a stiffening of

the bellows as opposed to an increase in bearing friction.

Tests are performed on saturated LHe with vapor pressures ranging from 27.3 to 880 torr, corresponding to temperatures of 2.05 K to 4.38 K. By the two-fluid model, SF concentrations reach as high as 25% at the lowest temperature attained. The lambda transition consistently occurs at 36 torr (2.16 K) in the system, inferred from the rapid and complete cessation of turbulence and rising He vapor bubbles observable in the view ports.

### 3.2 Calibration

Use of Eq. 3 requires knowledge of the HV-charger capacitance ( $C_{HC}$ ) and fixed capacitance ( $C_{CF}$ ) when the gap between these electrodes is set to its reference value at which the electrical measurements are made. The reference spacing is 5.0 cm, as given by the motor driver software. With the system full of LHe just below the lambda point, the HV electrode is grounded by closing the gap between it and the movable ground electrode. A digital capacitance bridge is connected between the upper tip of the air-vacuum feedthrough and the nearest point on the exterior of the (grounded) insulating vacuum chamber. Bridge readings are then recorded as the charger is moved back from the HV electrode.

Results are shown in Fig. 9. Data represent the parallel sum of the capacitances  $C_{HC}$  and  $C_{CF}$  (Fig 7). To extract separate values for these capacitances,  $C_{HC}$  is modeled as a parallel-plate capacitor and the data are fit the expression

$$C = C_{CF} + C_{HC} = C_{CF} + \frac{A}{z - z_0}. \quad (4)$$

Here,  $A$  is a constant,  $z$  is the electrode separation, and  $z_0$  is an offset reflecting the uncertainty in the absolute separation. The fit returns a value of  $132.2 \pm 0.2$  pF for  $C_{CF}$ . Using the values of  $A$  and  $z_0$  returned from the fit and substituting  $z = 5.0$  cm for the reference separation yields the reference value for  $C_{HC}$  of  $1.05 \pm .05$  pF. As  $C_{HC}$  is less than 1% of  $C_{CF}$  (and in any case  $C_{HC} \ll C_{MF}$ ), Eq. 3 reduces to

$$\Delta V_{HG} = \left( \frac{1}{C_{HC}} \right) \int i dt \quad (5)$$

where  $i$  is the output of the current amplifier.

An assessment of the leakage current from the HV electrode at a given HV-ground electrode gap (Sec. 3.5) requires a knowledge of the total capacitance

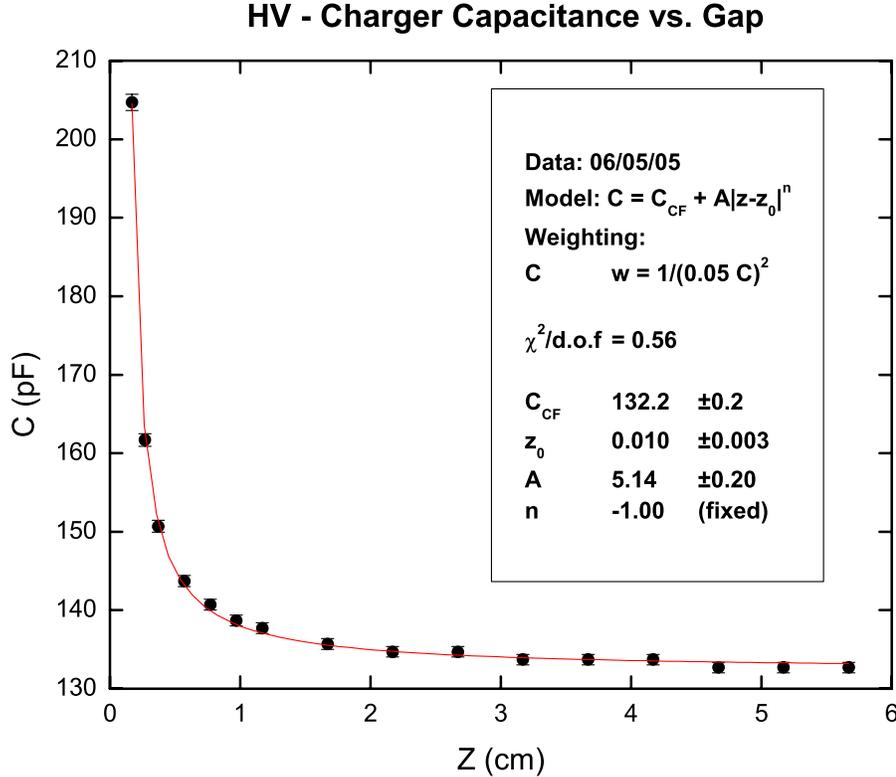


Fig. 9. Charger–HV electrode capacitance as a function of separation. A statistical error of 0.5% is assumed on each point. The legend shows the result of a least-squares fit.

of the HV electrode with respect to ground at the particular gap setting. This capacitance is very closely approximated by  $C_{HG} + C_{HF}$  in Fig. 7. With the bridge still connected as above, both the ground and charger electrodes are brought into contact with the HV electrode. Bridge readings are then recorded as the ground electrode is stepped back from the HV electrode. The data are shown in Fig. 10. This curve yields a direct measurement of the desired capacitance as a function of the gap.

### 3.3 Voltage Amplification and Breakdown Strength

Amplification tests are performed with an initial gap between the HV and ground electrodes of 2–3 mm. At this gap, the highest possible potential is established with the power supply. This is typically achieved after several attempts in which spark discharges occur across the gap at lower potentials. Presumably these discharges are initiated by sharp points and/or frozen contaminants on the electrode surfaces, and they decrease in frequency as contaminants are destroyed by successive sparks in a process analogous to the “conditioning” observed in vacuum–insulated systems. During tests with the initial gap set to a few cm, the HV electrode can usually be charged to the

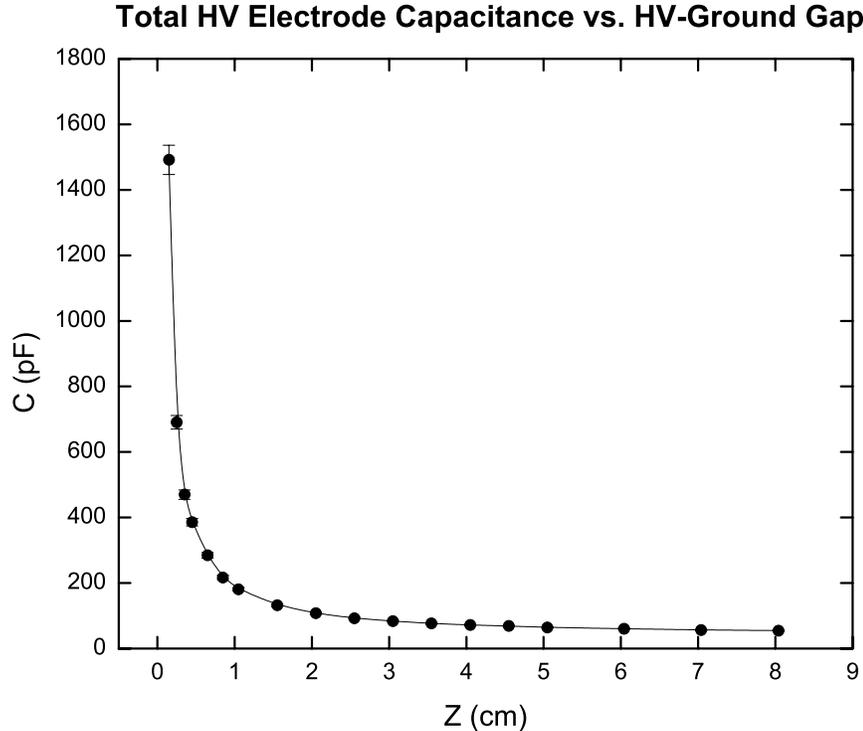


Fig. 10. Total HV electrode capacitance as a function of HV-ground electrode separation. A statistical error of 3% is assumed on each point. The line connecting the points is a spline interpolation.

full capacity of the power supply (50 kV) with the system full of LHe above or below the lambda point. This indicates that the vacuum-LHe feedthrough can withstand voltages 25% higher than its nominal breakdown rating in air when immersed in LHe.

Voltage amplification data are shown in Fig 11. Output of the current amplifier is plotted as a function of the time since the start of a data acquisition cycle. With the exception of a few transients, the current traces in Fig 11 remain at zero for the first few seconds after the data acquisition is started, consistent with no current flow—that is, no transfer of charge to the charger electrode—when the ground electrode is at rest. When the ground electrode retraction is begun (after approximately 10 s) the current immediately rises (for example, to about 10 nA in the case of Fig 11a). The current then slowly decays (for example, over the next 85 s in Fig 11a) as the retraction proceeds at constant velocity. In the limit of an ideal parallel-plate capacitor, the current would be expected to remain constant for a constantly increasing plate separation; the decay observed in Fig 11 is a consequence of the fixed capacitance between the HV electrode and ground ( $C_{HF} \sim 40$  pF, as inferred from bridge measurements). The current drops back to zero when the ground electrode retraction stops (for example, after 95 s, corresponding to a gap of 7.8 cm, in Fig 11a).

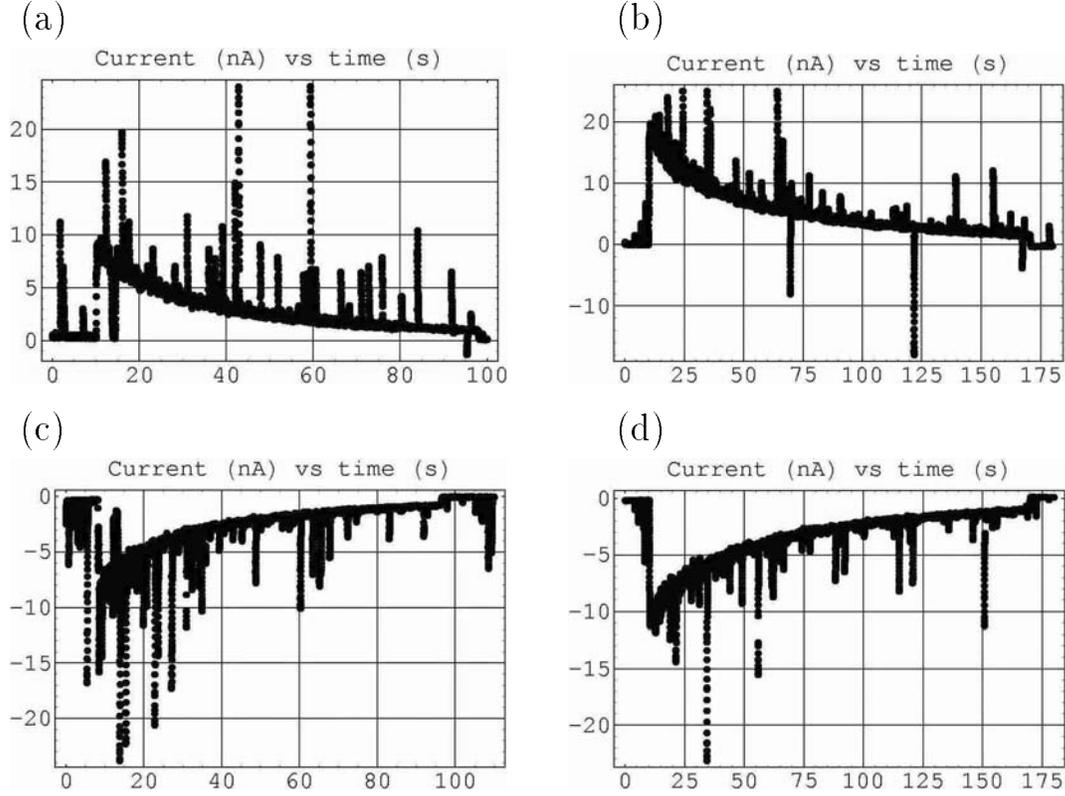


Fig. 11. Amplification data showing output of the current amplifier in nA vs. time in seconds. Data sets correspond to the largest voltages attained with the test system. In (a), the data are obtained with the LHe bath at 34.5 torr (2.14 K), an initial gap (visible in the transit) of 2.9 mm, and an initial potential of 13 kV at this gap. The ground electrode is retracted at 5.08 cm min<sup>-1</sup>. In (b), the LHe bath pressure is 880 torr (T = 4.38 K), the initial gap is 3.0 mm, the initial potential is 42 kV, and the electrode retracted at 2.54 cm min<sup>-1</sup>. In (c), the LHe bath pressure is 31.9 torr (T = 2.11 K), the initial gap is 3.0 mm, the initial potential is -11.5 kV, and the electrode retracted at 5.08 cm min<sup>-1</sup>. In (d), the LHe bath pressure is 654 torr (T = 4.06 K), the initial gap is 3.1 mm, the initial potential is -31 kV, and the electrode retracted at 2.54 cm min<sup>-1</sup>.

The total charge  $\Delta Q_C$  accumulated on the charger electrode, as the ground electrode is retracted, is computed from the sum

$$\Delta Q_C = \sum_n (t_{n+1} - t_n)(i_{n+1} + i_n)/2, \quad (6)$$

where  $t_n$  and  $i_n$  represent the time and current values of the  $n$ th point in the data set. A value for Eq. 5 is obtained by dividing this sum by  $C_{HC}$ , and the total voltage is found by adding the value of the initial potential between the plates. The voltage at any value of the electrode separation is found by truncating the sum in Eq. 6 at each time point and converting the time axis to electrode separation. The voltage as a function of separation derived from the

data in Fig. 11 is shown in Fig. 12. In each case, the range of values defined by the 1-sigma error bars is shown.

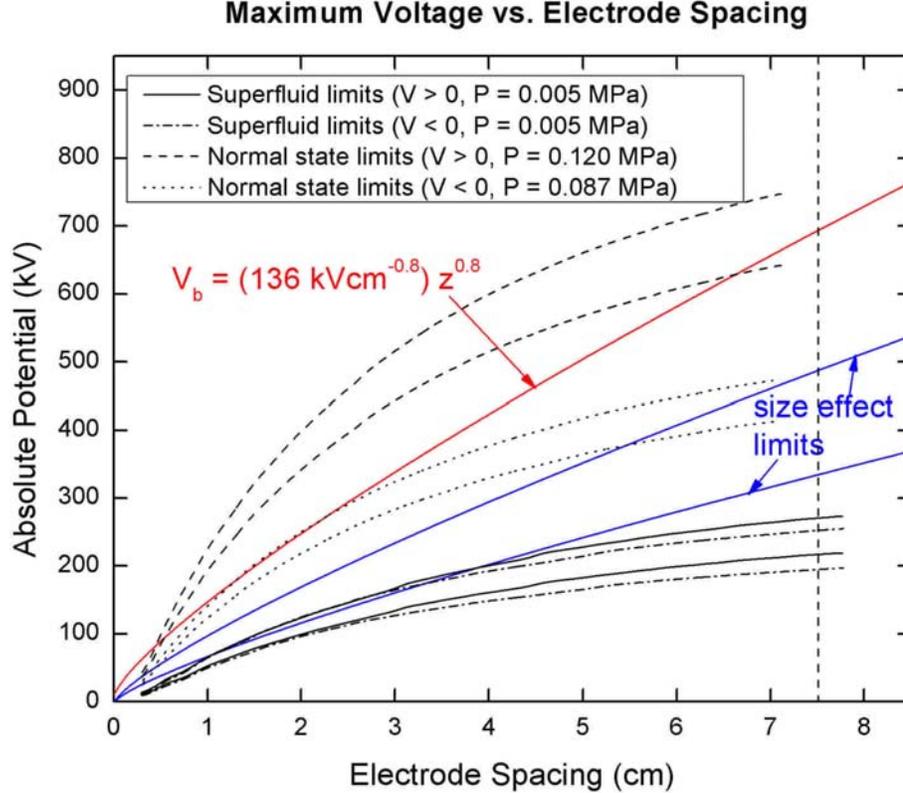


Fig. 12. Voltages obtained in HV test system as function of electrode spacing. The data curves are labeled only in the legend. The data curves define the range (as determined by the 1-sigma error bars) of the maximum voltages obtained in LHe, for positive and negative initial potentials, above and below the lambda point. The extrapolated breakdown curve and size effect breakdown estimates from Fig. 1 are also shown.

The extrapolated breakdown and size effect curves from Fig. 1 are also shown for reference. Direct comparison between the data and the extrapolated breakdown curves is misleading in that, first, the data curves represent the highest voltages successfully maintained in the system without breakdown during single, complete sweeps of the ground electrode. The shape of the data curves is determined by the capacitance of the high voltage electrode with respect to ground as the spacing changes, and not by breakdown events observed at each value of the spacing. As expected for the parallel plate geometry, the voltage increase is approximately linear with the spacing for the first 1-2 cm, then levels off in the presence of the large fixed capacitance. Second, the normal state data suggest that voltages larger than the dielectric strength measured in previous experiments are attained below 1 cm (see Fig. 1). Here it is important

to note that the normal state data (positive voltage) in Fig. 12 are obtained at a pressure of 880 torr. This is approximately 20% higher than for the data in Fig. 1 and, as described in the next section, dielectric breakdown in LHe is a strong function of pressure. Normal state data with negative voltage in Fig. 12 are obtained just above atmospheric pressure in the lab at Los Alamos and most closely approximate the conditions of the experiment in Fig. 1.

Three contributions to the error bars are considered. First, a 5% uncertainty results from the error in  $C_{HC}$ , as derived from the fit in Fig. 9. Second, the output from the current amplifier corresponding to zero current is observed to drift by as much as 0.1 nA over several tens of seconds, based on observations of the tails of the raw data plots (Fig. 11) corresponding to when the ground electrode is at rest. An average zero offset of this magnitude translates into a  $\pm 3\%$  shift in the summation in Eq. 6, and a corresponding shift in the measured voltage. The third (and usually the largest) effect is due to the transient spikes observed in the raw data traces. While it is unlikely that the transients represent an actual accumulation or loss of charge on the electrodes during amplification and can be ignored for the purpose of determining the voltage (see Sec. A below), the evidence as of this writing is anecdotal, therefore the effect of the transients is accounted for in the uncertainty. To determine the effect of the transients, the data sets in Fig. 11 are partitioned into 1 s time bins. The minimum absolute current is determined in each bin, and all individual points in a given bin with current values greater than 20% of the minimum are removed. Eq. 6 is used again to find the voltage vs. separation from the reduced data set, which is then subtracted from the value obtained from the original data set. For the case of positive initial potentials, removal of transients from the SF (normal state) data reduces the voltage by an average of 13% (6%).

The effect of the transients is positive (negative) in the case of positive (negative) initial HV electrode potential, so the contribution of the transients to the error bars is one-sided. At maximum electrode separation (7.8 cm for the measurement in SF and 7.2 cm for the measurement in normal state LHe), the largest positive voltages attained are  $240_{-14}^{+34}$  kV and  $688_{-41}^{+58}$  kV, respectively. The largest negative voltages are  $-215_{+13}^{-37}$  kV and  $-443_{+27}^{-31}$  kV, respectively. These values represent lower limits on LHe breakdown strength below and above the lambda point at large electrode separations; the stressed LHe volumes are 12.8 liters for SF and 11.8 liters for the normal state.

### 3.4 Pressure Dependence of Breakdown Strength

The maximum voltages attainable in the HV test system below the lambda point are about 30-50% of those attained above, and are roughly 60% of the

design goal for the EDM experiment. It is unlikely that the reduced performance of the HV test system below the lambda point is due exclusively to an intrinsic property of the SF component of the LHe. This is illustrated in Fig. 13, which shows the maximum voltages attained in the system at various pressures and temperatures.

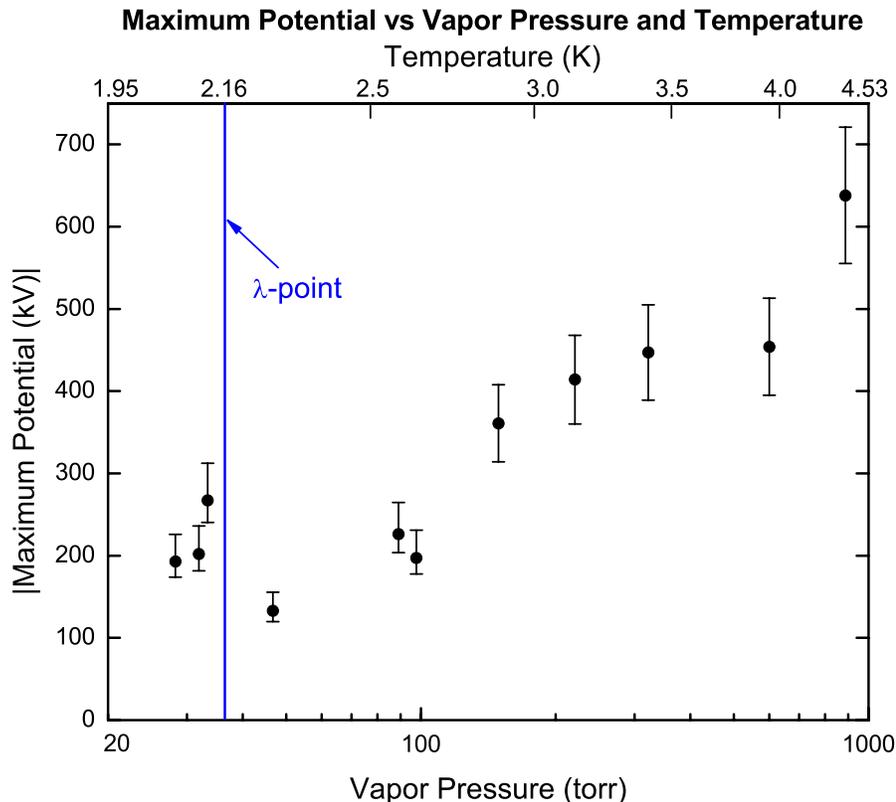


Fig. 13. Maximum voltages attained in HV test system over 12 hour period as a function of pressure and temperature. Statistics below lambda point are highest values measured in 0.05 K bins above 27.3 torr (2.05 K) obtained in a series of many tests over a 6 hour period. Remaining data are obtained over subsequent 6 hours in which system is warmed continuously by the  $\sim 2$  W heat load.

From the figure, comparable maximum voltages are attainable in the system both above and below the lambda point at vapor pressures of 100 torr and below. This is consistent with several previous reports of comparable breakdown strength of saturated normal state and SF LHe [6]. While the data above the lambda point were taken over the course of a 6 hour warm up period, this period occurred immediately after an interval of comparable duration in which the system was kept below the lambda point and during which many breakdown tests were performed. Therefore it is unlikely that the observed improvement with pressure is the result of conditioning. It seems reasonable that, as in at least one previous experiment [6], some of the resistance against breakdown observed in the system near atmospheric pressures can be recov-

ered by pressurizing a sealed volume of LHe kept below the lambda point. Based on the compressibility of SF LHe ( $10^{-7} \text{ Pa}^{-1}$  [10]), the pressurization would only require a variable volume of a few liters in series with the HV test system main volume and is a possible design improvement in the near future.

### 3.5 Leakage Current Limits

Stability of the voltage between the electrodes over time is assessed by establishing the highest possible charge on the electrodes at maximum separation under the desired conditions, waiting for the longest possible period under which the conditions can be maintained, and re-measuring the charge at the end of this period. The initial charge is measured in the usual way (Eq. 6) during the outward stroke of the ground electrode; the charge remaining after the holding period is measured by applying Eq. 6 to the data obtained as the ground electrode is returned to its original gap. The difference in charge measured over the holding period is then expressed as a leakage current. Data used for leakage current measurements in SF and normal state LHe are shown in Fig. 14

The leakage current from the HV electrode ( $i_{HV}$ ) is determined from the expression for the voltage, multiplied by the total capacitance of the electrode at maximum spacing ( $C_{HV} \approx C_{HG} + C_{HF}$  in Fig. 7) and divided by the holding time  $\Delta t$ :

$$i_{HV} = \frac{C_{HV}}{C_{HC}} \frac{\delta Q_C}{\Delta t}. \quad (7)$$

Here,  $\delta Q_C$  is the *difference* in the charge accumulation determined from the data corresponding to the outward and inward strokes of the ground electrode in Fig 14. From Figs. 14a and b, this difference as measured below the lambda point is consistent with zero, when accounting for the uncertainties associated with amplifier zero drift and transients. The 95% C. L. upper limit on the charge difference is 14 nC. The time  $\Delta t$  between the outward and inward strokes is  $1009 \pm 6$  s, limited by concern over the liquid level dropping below the top edges of the electrodes after several hours of tests. From Figs. 14c and d, the charge difference as measured at atmospheric pressure is also consistent with zero; the 95% C. L. upper limit is 160 nC. In this case the system had been topped off with LHe just before the first measurement and was left overnight, resulting in time  $\Delta t = 41520 \pm 600$  s. The electrode capacitance at maximum separation (again, 7.8 cm for the SF data and 7.2 cm for the normal state) is found from the curve in Fig. 10 to be  $C_{HV} = 55 \pm 2$  pF and  $57 \pm 2$  pF, respectively.

Using the above measurements in Eq. 7 results in 95% C. L. upper limit

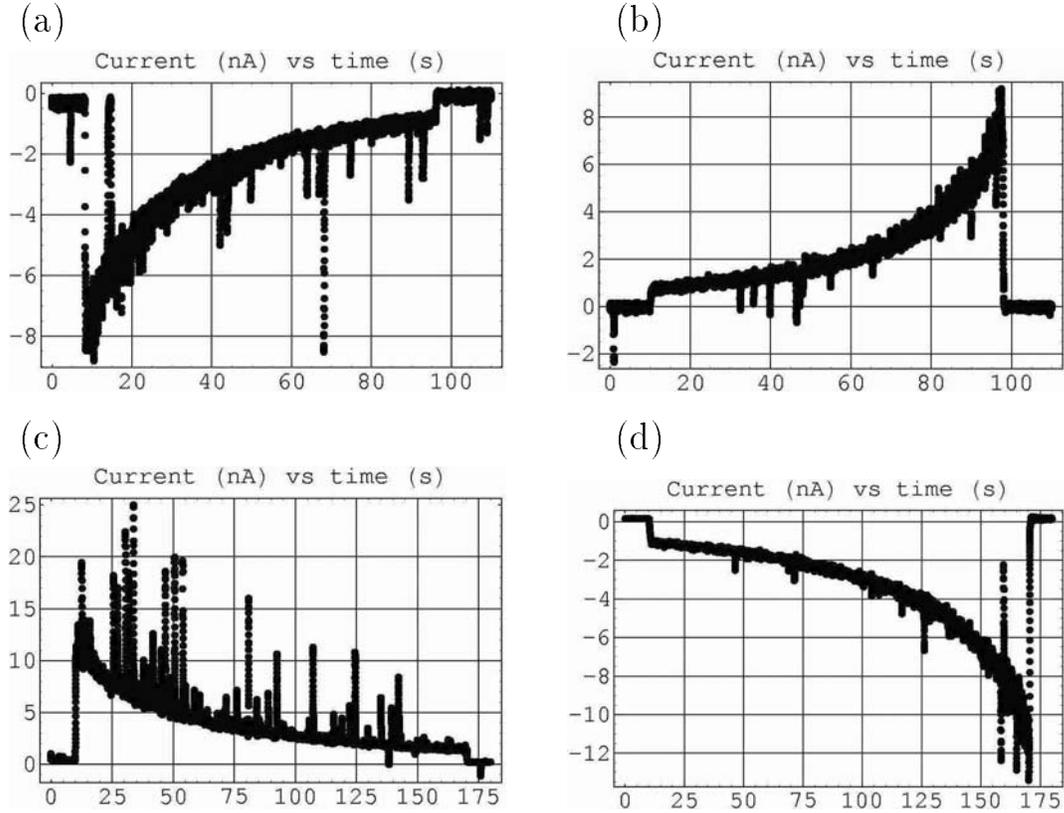


Fig. 14. Output of the current amplifier in nA vs time in seconds for leakage current assessment. In (a), the data are obtained with the LHe bath at 27.3 torr (2.05 K), an initial gap (visible in the transit) of 2.9 mm, and an initial potential of -6 kV at this gap. The ground electrode is retracted at  $5.08 \text{ cm min}^{-1}$ . Fig. (b) shows data from the return stroke of the ground electrode after a holding time of 16.8 min at the maximum gap of 7.8 cm; the LHe bath pressure is 30.0 torr ( $T = 2.09 \text{ K}$ ), and the electrode is returned at  $5.08 \text{ cm min}^{-1}$ . In Fig. (c), the LHe bath pressure is 600 torr ( $T = 3.98 \text{ K}$ ), the initial gap is 3.0 mm, the initial potential is 29 kV, and the electrode is retracted at  $2.54 \text{ cm min}^{-1}$ . Fig. (d) shows data from the return stroke of the ground electrode after a holding time of 11 hr and 32 min at the maximum gap of 7.2 cm; the LHe bath pressure is 600 torr ( $T = 3.98 \text{ K}$ ), and the electrode is returned at  $2.54 \text{ cm min}^{-1}$ .

estimates of the leakage current of 733 pA for the HV electrode in SF and 169 pA in normal state LHe. While these results are consistent with zero, the large uncertainty on the SF measurement allows for values near the 1 nA design limit for the EDM experiment and is of some concern. These results are however, preliminary, and provision for several hours of holding time below the lambda point will be made in subsequent tests of the system.

### 3.6 Neutron Radiation Effects

The Spallation Neutron Source will use a beam of high energy protons (nominally 1 GeV with a 60 Hz repetition rate) directed at a liquid mercury target to produce fast neutrons which will be partially moderated by a liquid hydrogen cell. The EDM experiment is scheduled to be installed on a dedicated beam line with a neutron momentum centered at 8.9 Å (the optimum momentum for the production of UCN via downscattering in SF LHe.) While the series of monochromators and frame definition choppers used to select the momentum is expected to provide a narrow bandwidth, there is some concern that performance of the HV and other systems in the EDM experiment will degrade in the presence of a fast neutron background. To check the operation of the HV test system under extreme background conditions, charging and amplification tests are performed in the presence of a 7 Ci PuBe neutron source.

The charging test (at atmospheric pressure) is performed in three phases. With the gap between the electrodes fixed at 3 mm, the HV electrode is charged to the maximum possible potential in the absence of the source. The charging is repeated with the source placed next to the exterior of the insulating vacuum system, behind a 2 cm thick slab of polyethylene, at a point approximately 50 cm from the center of the front surface of the HV electrode. Finally, the charging is repeated once more with the polyethylene slab removed. The maximum voltages attained, together with the estimated neutron flux for each phase, are shown in Table 4. The results are consistent with a slight improvement of the charging capability of the system in the presence of an increasing fast neutron background. However, the test began less than 1 hr after a refill of the LHe volume and after a few minutes of conditioning, so the slight improvement could also be due to some extra conditioning.

With the source still in place, the system is again charged to 30 kV and an amplification test is performed. The electrodes are held at maximum separation (7.2 cm), but only for a few minutes in the interest of reducing activation of the system components. The voltage attained at this separation is  $475_{-29}^{+38}$  kV with no anomalous behavior observed, consistent with the performance of the system at atmospheric pressure in the absence of neutron radiation.

For the amplification tests below the lambda point, the PuBe source is placed in the same location but left on top of the polyethylene slab, resulting in a neutron flux similar to that in the third row of Table 4. Tests at both positive and negative initial voltages are performed; data corresponding to the outward stroke of the ground electrode with positively charged HV electrode are shown in Fig. A.1a. Voltages obtained at maximum electrode separation are  $259_{-16}^{+52}$  kV and  $-274_{+16}^{-55}$  kV. These values are consistent with nominally better performance than in the absence of the fast neutron background (Fig. 12).

Table 4

Neutron radiation effects on HV electrode charging. The HV-ground gap is set to 3.0 mm, LHe bath pressure = 600 torr ( $T = 3.98$  K). Tests began  $\sim 30$  min after LHe fill, with  $\sim 5$  min prior conditioning.

<i>n-flux in gap</i>	<i>Breakdown V (kV)</i>	<i>Comments</i>	<i>Time (min)</i>
(Background)	$30 \pm 1$	no source	0.0
$10^6 \text{ s}^{-1}$ , $E \sim 1 \text{ MeV}$ with 10% 1 keV admixture	$34 \pm 2$	source behind 2 cm polyethy- lene	3.0
$10^6 \text{ s}^{-1}$ , $E \sim$ 1 MeV	$36 \pm 2$	polyethylene re- moved	7.0

However, the pervasive transients observed in the data are a concern, and the large uncertainty associated with them leaves the repeatability of these results in question.

#### 4 Conclusions and Outlook

A prototype HV amplification system, consisting of a large, variable parallel-plate capacitor has been constructed for a proposed neutron EDM experiment in SF LHe. The system has been used to amplify voltages in the range of about 10 kV to 240 kV or greater across an electrode gap of 7.8 cm in SF LHe. This is roughly 60% of the design goal for the EDM experiment, which will have electrodes with a comparable gap, and represents a lower limit on the dielectric breakdown strength of SF LHe at large volumes. These results are not appreciably changed in the presence of a high background flux of fast neutrons. Upper limits to detectable leakage currents have been set at about 750 pA, nominally tolerable in the final experiment. Considerable improvement in voltage tolerance and leakage current is observed with the system full of normal state LHe at 4 K, performance that will likely be recoverable at lower temperatures by pressurizing the LHe bath. Additional statistics at low temperatures with highly polished electrodes will be acquired to establish a stable operating voltage, and to better understand the conditions for bubble formation which is likely responsible for measurement noise as well as reduced breakdown strength. Electric breakdown studies of candidate materials for the EDM experimental test cells, using samples mounted behind the HV electrode in the prototype system, are also anticipated in the near future.

## Acknowledgments

The investigators would like to thank V. Sandberg of Los Alamos National Laboratory for suggesting the voltage amplification method, and J. Jarmer of Los Alamos and J. Price of the University of Colorado for advice on cooling the large LHe volumes in the HV test system to below the lambda point.

## A The Effect of Transients

The transient current signals in the data traces (Figs. 11, 14, A.1) have considerable influence on the uncertainty of the measured LHe properties. This section summarizes the observed characteristics of the transients and proposes a model for their explanation.

An expanded view in time of a transient is shown in Fig. A.1b. Typical transients have an amplitude of about 1-25 nA. The usual rise time (10%-90%), FWHM, and decay times are about 20 ms, 100 ms, and 150 ms, respectively. Observations relating to transient formation include:

- (1) Transient signal shape (amplitude, rise and decay times, FWHM) does not change significantly with helium vapor pressure.
- (2) Transients are almost exclusively positive (negative) when the HV electrode is positively (negatively) charged (compare Figs. 11a and 11c).
- (3) Transient density (number per unit time) increases at lower helium vapor pressures (compare Figs. 11a and 11b).
- (4) Transient density increases with applied field, at least at low vapor pressure (compare Figs. 14a and b, and 11a and c).
- (5) Transient density at low vapor pressure increases further in the presence of neutron radiation (compare Figs. 11a and A.1a).

Since the amplification signal is essentially DC, HV data are taken with the input filter on the current amplifier set to low-pass. Specifically the cutoff frequency is set to 3 Hz and the roll-off to 12 dB/octave. To simulate these conditions, tests are performed with a signal generator connected to the input of the amplifier, with the same filter settings, through a 20 M $\Omega$  series resistor. Output signals similar in rise time, FWHM, and decay time to the transients in the HV data can be obtained with square pulses 10 ms long and separated in time by a few hundred ms. The pulse amplitude is attenuated by about a factor of 5. It is therefore probable that the transient signal shape in the HV data is determined largely by the amplifier input filter. The actual transient phenomena are likely significantly faster (at most a few ms) and larger (up to a few tens of nA).

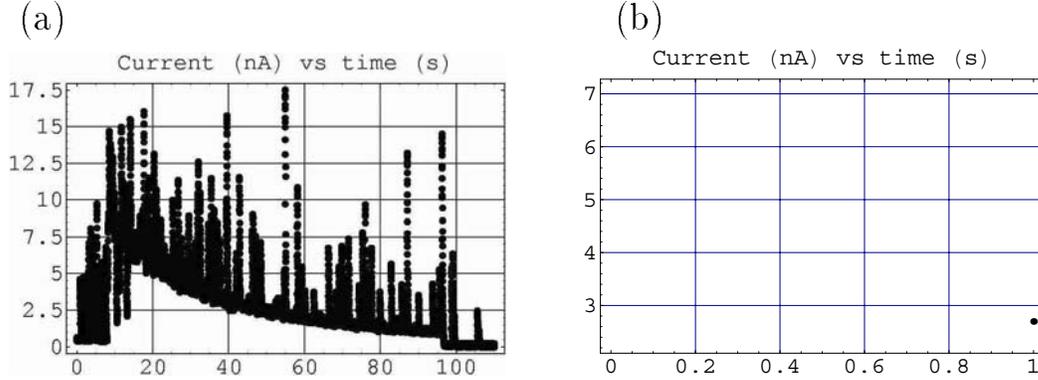


Fig. A.1. Output of the current amplifier in nA vs time in seconds illustrating transient effects. Fig. (a) shows an amplification test in the presence of a PuBe source. The LHe bath pressure is 33.8 torr ( $T = 2.13$  K), the initial gap is 2.8 mm, the initial potential is 13 kV, and the electrode retracted at  $5.08$  cm  $\text{min}^{-1}$ . Fig. (b) is a 1 s time slice of an amplification data trace, showing a typical transient.

The last three observations enumerated above suggest that transients increase under conditions progressively more favorable for bubble formation on the cathode electrode. Bubbles with radii on the order of  $r \sim 0.1\text{--}1$  mm are observed to form on the ground electrode during the initial charging of the system before an amplification test. They usually appear after a positive potential of 10 kV or more has been established across the 2–3 mm gap, though detailed observations of bubble formation and the conditions under which it occurs or is enhanced have yet to be made.

The formation of bubbles in the gap can lead to a coincident increase in the observed current at a particular gap voltage. This is because the dielectric constant of helium vapor or vacuum ( $\kappa = 1.00$ ) is lower than that of the normal state or SF liquid ( $\kappa = 1.05$ ); bubble formation leads to a decrease in the HV–ground electrode capacitance. To estimate this effect, the change in capacitance  $\Delta C$  due to the formation of a bubble of radius  $r$  is  $\Delta C = 4\pi\epsilon_0 r \Delta\kappa$ . For bubbles of radius  $r \sim 0.1\text{--}1$  mm,  $\Delta C = 0.5\text{--}5$  fF. A bubble protruding 0.1–1 mm from the ground electrode in a typical field between in the gap of  $20$  kV  $\text{cm}^{-1}$  sits at an average potential of 200–2000 V. While the time evolution of bubble formation in the system has not been studied, the formation of one of the larger bubbles on a time scale of  $\Delta t \leq 1$  ms would lead to a current spike on the order of  $V\Delta C/\Delta t \geq 10$  nA, consistent with the amplitude of the observed transients. The sign of this current signal follows the sign of the voltage, also consistent with observations.

While this model provides an ostensible explanation of the transients, one drawback is that current signals of opposite sign, associated with the recovery of the capacitance once the bubbles detach from the electrode and drift out

of the gap, are expected to be observed as well. A lower limit on the average escape time of a bubble from the gap can be estimated from the buoyant and drag forces on the bubbles in the liquid.

Once detached from the electrode, bubbles float toward the surface of the LHe under the influence of the buoyant force  $F_b = V_b \rho_l g$ , where  $V_b$  is the bubble volume,  $\rho_l$  is the liquid density (assumed constant through the bath depth at  $1.3 \times 10^2 \text{ kg m}^{-3}$ ) and  $g$  is the acceleration due to gravity. For bubbles with  $r = 1.0 \text{ mm}$ , this force is initially about  $5 \text{ }\mu\text{N}$ .

Motion of the bubble up through the liquid is opposed by a drag force  $F_d$ , as well as an added-mass force  $F_{m'}$  induced by the displacement of the fluid surrounding the bubble as it rises [11]. For the case of spherical bubbles in a viscous fluid,

$$F_d = 12\pi\eta r \mathbf{v}; F_{m'} = \frac{V_b \rho_l}{2} \mathbf{a}. \quad (\text{A.1})$$

Here,  $\eta = 1.6 \times 10^{-6} \text{ Pa s}$  is the viscosity of the normal-state component of the LHe at 2.1 K, and  $\mathbf{v}$  and  $\mathbf{a}$  are the bubble velocity and acceleration.

Setting the buoyant force equal to the sum of the drag and added-mass forces, and neglecting the bubble mass, the equation of motion for a rising bubble reduces to:

$$\mathbf{a} - 2g + \frac{18\eta}{r^2 \rho_l} \mathbf{v} = 0. \quad (\text{A.2})$$

Due to the low density of the LHe, the hydrostatic pressure at any point along the electrode surfaces is determined almost exclusively by the vapor pressure above the bath, even for the lowest vapor pressures ( $\sim 30 \text{ torr}$ ) attained. Therefore the radius of a rising bubble remains essentially unchanged, and the coefficient of the  $\mathbf{v}$  term is constant. For a bubble with  $r = 1 \text{ mm}$ , the coefficient is about  $0.1 \text{ s}^{-1}$ , implying that a rising bubble does not reach an appreciable fraction of its terminal velocity for  $\sim 10 \text{ s}$  and accelerates out of the gap with  $\mathbf{a} \sim 2g$ . Assuming on average that bubbles form near the middle of the electrode, bubbles have to float up from rest through about 20 cm of LHe to escape the gap; the average escape time is at least 100 ms.

The recovery of the capacitance presumably occurs as the bubble drifts out through the fringe field near the rounded edge of the electrode, over a time period shorter than but on the order of the escape time. If this interval is 10 ms or greater, the observed (opposite-sign) current transient for a bubble escaping the gap would be at most about 1 nA, just above the resolution determined by the noise in the readout (see, for example, the baseline in Fig. A.1b). This

suggests that only the largest bubbles escaping the gap would have a nominally visible effect, though the full implication for the model as to whether bubbles must remain attached to the electrodes (or must otherwise be prevented from a fast escape from the gap) is unclear.

Nevertheless, if correct, the model suggests that the transients do not correspond to an actual accumulation of charge during amplification and can be removed from the data sets to assess the actual voltages attained in the HV system. However, the model is based only on a few casual observations during initial operation of the system. More careful studies of the actual signal profiles of the transients, as well as of bubble formation, size, and number density as a function of time, vapor pressure, applied voltage and electrode surface roughness will need to be carried out in the near future.

## References

- [1] Smith, J. H., Purcell, E. M., and Ramsey, N. F., Phys. Rev. 108 (1957) 120.
- [2] Khriplovich, I. B., and Lamoreaux, S. K., CP Violation Without Strangeness (Berlin, Springer Verlag, 1997).
- [3] Harris, P. G., et al., Phys. Rev. Lett. 82 (1999) 904.
- [4] Golub, R. and Lamoreaux, S. K., Phys. Rep. 237 (1994) 1.
- [5] EDM Collaboration, "A New Search for the Neutron Electric Dipole Moment," Los Alamos Report LA-UR 02-2331 (2002).
- [6] Gerhold, J., Cryogenics 38 (1998) 1063.
- [7] Gerhold, J., Dielectric properties of cryogenics, in Seeber, B., Handbook of Applied Superconductivity 1 D, Cooling Technology for Superconductors, Inst. of Phys., Bristol, 1998.
- [8] Lamoreaux, S. K., Phys. Rev. A 53 (1996) 3705.
- [9] Sushkov, A. O., et al., Phys. Rev. Lett. 93 (2004) 153003, physics/0403143.
- [10] Keller, W. E., Helium-3 and Helium-4 (New York, Plenum Press, 1969).
- [11] Lamb, H., Hydrodynamics, 6th Ed. (New York, Dover, 1945) 124.